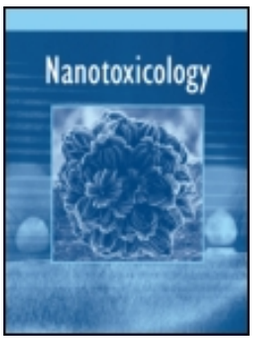

Nanotoxicology

ISSN: 1743-5390 (Print) 1743-5404 (Online) Journal homepage: https://www.tandfonline.com/loi/inan20

Using gold nanorods core/silver shell nanostructures as model material to probe biodistribution and toxic effects of silver nanoparticles in mice

Jie Meng, Yinglu Ji, Jian Liu, Xuelian Cheng, Hua Guo, Weiqi Zhang, Xiaochun Wu & Haiyan Xu

To cite this article: Jie Meng, Yinglu Ji, Jian Liu, Xuelian Cheng, Hua Guo, Weiqi Zhang, Xiaochun Wu & Haiyan Xu (2014) Using gold nanorods core/silver shell nanostructures as model material to probe biodistribution and toxic effects of silver nanoparticles in mice, Nanotoxicology, 8:6, 686-696, DOI: 10.3109/17435390.2013.822593

To link to this article: https://doi.org/10.3109/17435390.2013.822593

Nanotoxicology, Month 2014; Early Online:686–696

ISSN: 1743-5390 print / 1743-5404 online
DOI: 10.3109/17435390.2013.822593

informa
healthcare

Using gold nanorods core/silver shell nanostructures as model material to probe biodistribution and toxic effects of silver nanoparticles in mice

Jie Meng[1], Yinglu Ji[2], Jian Liu[1], Xuelian Cheng[1], Hua Guo[1], Weiqi Zhang[1], Xiaochun Wu[2], & Haiyan Xu[1]

[1]*Institute of Basic Medical Sciences, Chinese Academy of Medical Sciences & Peking Union Medical College, Beijing, P. R. China and* [2]*CAS Key Laboratory of Standardization and Measurement for Nanotechnology, National Center for Nanoscience and Technology, Beijing, P. R. China*

Abstract

The aim of this work was to probe the biodistribution and toxic effects of silver nanoparticles (NPs) with powerful antibacterial and anti-virus activities. For this purpose, novel silver NPs with gold nanorod (NR) core and silver shell (Au@Ag NRs) were developed and employed as a model material. The inner gold core provided an excellent internal reference for tracking the NRs *in vivo*. After subcutaneous injection of Au@Ag NRs, silver and gold contents in the subcutis and organs were examined by inductively coupled plasma mass spectrometry at different time points within 28 days. Histological analysis, physiological function and complement faction 3 (C3) and 5a (C5a) measurement were performed over time to reveal the toxic effect of Au@Ag NRs *in vivo*. Experimental results showed that majority of the Au@Ag NRs remained in the injection site except for a small amount migrating into the lymph nodes. The silver shell was dissolved in the subcutaneous tissue and released silver ions rapidly, which resulted in detectable silver accumulation in most of the organs. The accumulated silver ions in the kidney not only interacted with the kidney cells membrane but also induced a rapid increase of complement fraction C3 followed by a significant consumption and C3a and C5a production significantly in the serum, which resulted in kidney oxidative damage and eventually led to the morphological changes and filtration function impairment of the glomerulus. The released silver ions also caused oxidative injury of subcutaneous tissue in the injection site.

Keywords: silver nanoparticles, biodistribution, kidney, subcutaneous administration, complement activation

Introduction

Silver nanoparticles (NPs) have been well recognised as one class of much more powerful antibacterial materials and exhibited stronger beneficial effect on infection than conventional silver compounds (Singh et al. 2012). Based on this performance, silver NPs have been applied in various fields in recent years, not only in the household products such as being fillers in food package, clothing, socks, infant products and electronic home appliances (Singh et al. 2012; Sondi & Salopek-Sondi 2004; Cohen et al. 2007; Ahamed et al. 2010), but also in health-care products, typical examples including coatings for medical devices and wound-care products (Johnston et al. 2010; Wijnhoven et al. 2009; Edwards-Jones 2009; Chaloupka et al. 2010).

As the exposure of silver NPs to human and environment is rapidly increased, large amounts of experimental evidence of strong acute cytotoxicity exerted by the silver NPs have raised serious concern and arguments on their safety (Johnston et al. 2010). Upon cellular exposure, the toxic effects mainly include affecting cell cycle (Lee et al. 2011; Austin et al. 2011) and causing cell apoptosis through oxidative damage (Hackenberg et al. 2011; Sanpui et al. 2011; Nallathamby & Xu 2010; Li et al. 2010; Miura & Shinohara 2009; Piao et al. 2011a; Teodoro et al. 2011). The possible signalling pathways involved in the mechanisms for the resulting cellular damages mainly included Akt and Erk (Comfort et al. 2011), Nrf2 (Kang et al. 2012; Piao et al. 2011b), GDNF/Fyn kinase (Braydich-Stolle et al. 2010) and nuclear factor-kappa B (Eom & Choi 2010). Experimental results *in vivo* have been limited in literature and unresolved issues remain. It was reported that repeated intravenous administration resulted in silver accumulation mainly in liver, spleen and lung, and to a lower extent into kidney, heart, brain and testes (Lankveld et al. 2010). Orally administrated silver NPs were reported to induce inflammatory responses (Park et al. 2010) and accumulated in the kidney (Kim et al. 2009) and brain (van der Zande et al. 2012). Some group reported that dose-dependent histopathological abnormalities were seen in the skin, liver and spleen of

Correspondence: Haiyan Xu, Institute of Basic Medical Sciences, Chinese Academy of Medical Sciences & Peking Union Medical College, Beijing 100005, P. R. China. E-mail: xuhy@pumc.edu.cn and Xiaochun Wu, CAS Key Laboratory of Standardization and Measurement for Nanotechnology, National Center for Nanoscience and Technology, Beijing 100190, P. R. China. E-mail: wuxc@nanoctr.cn

(Received 23 January 2013; accepted 2 July 2013)

male guinea pigs exposed to the AgNPs in dermal acute and subchronic studies (Korani et al. 2011), while others suggested that colloidal AgNPs were relatively safe when administered to oral, eye and skin of the animal models for short period of time (Maneewattanapinyo et al. 2011).

Several groups proposed that silver NPs released silver ions (Ag^+) from their surface (Damm & Munstedt 2008; Zook et al. 2011; Kittler et al. 2010) resulting in Ag^+ exposure of the bacteria (Babu et al. 2011; McQuillan et al. 2012). Alvarez's group suggested that Ag^+ released from AgNPs was the definitive molecular toxicant to the bacteria, and the Ag^+ release could be controlled possibly through manipulation of oxygen availability, particle size, shape and/or type of coating (Xiu et al. 2012). Nevertheless, the actual mechanism of toxicity in animals is largely unknown. It has been challenging of how to identify the toxicity from silver ions, or silver NPs themselves, or both, mainly due to the complexity of the silver NPs dissolution and the lack of measurement technologies to identify sliver ions or silver NPs. Inductively coupled plasma mass spectrometry (ICP-MS) is widely and mostly applied to detect silver content in tissues or cells; however, it is not possible for ICP-MS to determine whether the detected silver is particulate or in silver ion.

Here we prepared a novel nanostructured silver material as a model for investigating silver NPs toxicity *in vivo* through subcutaneous injection. The novel material is silver nanorods (NRs) templated by gold core with well-defined size and shape as well as high stability in the aqueous solution (Xiang et al. 2008) (for simplicity, we termed them as Au@Ag NRs). Gold is quite stable in physiological conditions, while silver can dissolve and release silver ions that may diffuse to organs. It is not possible to determine whether the detected silver is in particle status or in silver ions by ICP-MS. The benefit of using Au@Ag NRs is that the gold cores are inert in biological environment and can act as an internal reference to evaluate the dissolution of the silver shell. For instance, if Au and Ag are both present in the tissue or organ, it means Ag is still associated with the Au core, and the Au@Ag NR particles themselves move to the tissue or organ. Otherwise, if only Ag content is detected and no gold content is present in the tissue or organs, the silver content should be attributed to Ag ions that are released from the Au@Ag NRs. Additionally, the original ratio of Ag to Au in the NR is fixed. By detecting the ratio variation in the subcutaneous tissue of the injection site, we can determine whether the silver dissolves from Au@Ag NRs. Hence, the novel nanostructured silver material will allow us to track and identify the Au@Ag NRs biodistribution and toxicity mechanism to organs. Another benefit is the well-defined shape and size of Au@Ag NRs, so it can be identified easily in the biological environment.

The reason of choosing subcutaneous administration is to simulate the serious burn wound in exposure to the wound dressing containing silver NPs. In deep wound or serious burn, epidermal and dermal tissue would be damaged and subcutaneous tissue is exposed to wound dressings directly, where plenty of blood vessels exist as well as cells. Although there are intensive interests in the uses of silver NPs for burns and wound dressings, potential detrimental outcomes or risks for humans with serious burns or deep wounds as well as for animals' exposure remain an open question. Regarding the above situation, our concerns are particularly with the influence of silver NPs on the subcutis and kidney, because kidney is the first target organ of heavy metal toxicity (Florea & Busselberg 2006).

We showed (as shown in Scheme 1) that majority of the subcutaneously administrated Au@Ag NRs aggregated in the injection site except for small part of them migrating into the lymph nodes. The Au@Ag NRs were dissolved in the subcutaneous tissue and released Ag^+ rapidly, which resulted in detectable silver accumulation in most of the organs. The Ag^+ caused oxidative damage to the glomerulus basement membrane as well as the subcutaneous tissues around the injection site.

Materials and methods

Preparation and characterisation of gold NRs core/silver shell nanostructures coated by poly sodium-p-styrene sulphate

The preparation of gold NRs core/silver shell nanostructures coated by poly sodium-p-styrene sulphate (PSS) was described in our previous study (Xiang et al. 2008). In brief, gold NRs were synthesised by a seed-mediated method by adding gold (Au) seeds to growth solution which were prepared by mixing cetyl trimethylammonium bromide (CTAB), $HAuCl_4$, $AgNO_3$, H_2SO_4 and ascorbic acid (AA) together. After concentration and purification, gold NRs were added to 50 ml 0.1 M CTAB aqueous solution containing AA (550 µl, 0.1 M), $AgNO_3$ (2 ml, 0.01 M) and NaOH (1.4 ml, 0.2 M). After shaking and incubation, the gold NRs core/silver shell nanostructures were obtained, centrifuged and redispersed in water, followed by adding PSS. After mixing for 3 h, the solution was centrifuged and redispersed in the desired volume and gold NRs core/silver shell nanostructures coated by PSS were obtained, termed as Au@Ag NRs in the present work. Concentration of Ag and Au in the resulting solution was determined by ICP-MS. Briefly, Au@Ag NR suspensions of 50 µl were added to a mixture of 6 ml concentrated nitric acid, 2 ml hydrochloric acid and 0.5 ml H_2O_2, followed by a microwave treatment of 20 min at 190°C, 70 bar. Microwave can provide a high-temperature, high-pressure environment that accelerates the dissolution of Au@Ag NRs in the acids. Upon cooling, the solutions were further diluted by adding purified water to a total volume of 40 ml. Subsequently, samples were measured using ICP-MS instrument (Thermo ICP-MS XII instrument, ThermoFisher).

The morphology of Au@Ag NRs was observed using a transmission electron microscope (TEM, Tecnai F30). The samples were prepared by dropping 10 µl of Au@Ag NRs suspension on Cu grid and drying in air. The absorption spectra of the Au@Ag NRs suspensions were recorded on a PerkinElmer UV–vis/NIR spectrophotometer (Lamdba 950). Zeta potential and hydrodynamic diameter of Au@Ag NRs suspension were measured with Zetasizer Nano ZS90 (Malvern instruments) at room temperature.

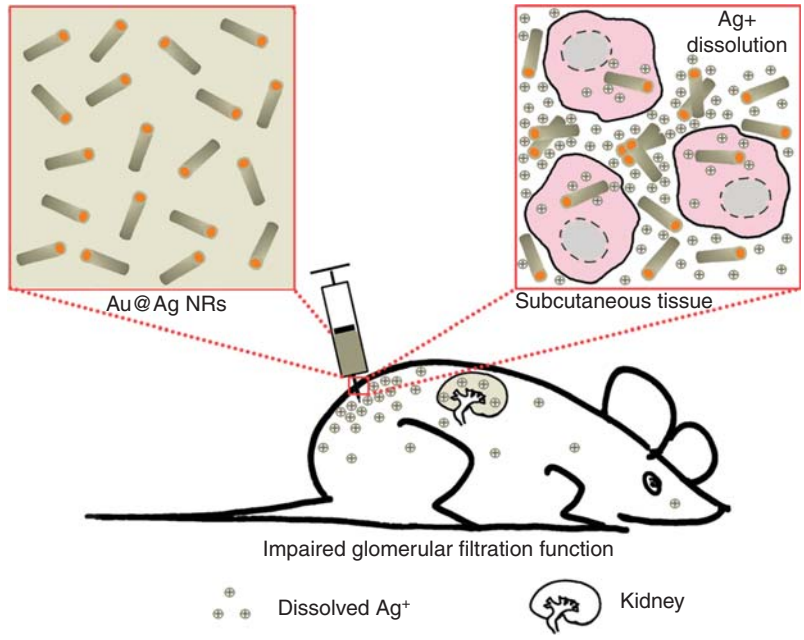

Scheme 1. A schematic diagram of *in vivo* toxicity studies for Au@Ag NRs subcutaneously injected to mice. Majority of Au@Ag NRs aggregated in the injection site while Ag^+ ions were rapidly released and distributed in most of the organs, which resulted in the injury of kidney as well as subcutaneous tissues.

Subcutaneous injection of Au@Ag NRs to BALB/c mice

Female BALB/c mice of 6–8 weeks old were maintained in the Experimental Animal Center at the Institute of Basic Medical Sciences, Chinese Academy of Medical Sciences (Beijing, China) under specific pathogen-free conditions. The mice were fed autoclaved water and food pellets. All the animal experiments reported herein were carried out in compliance with the national regulation governing animal experiments. Animals were acclimatised to laboratory conditions for 1 week prior to experiments. Following acclimatisation, mice for Au@Ag NRs exposure received subcutaneous injections of Au@Ag NRs of aqueous suspension in the neck area, and the injected volume per mouse was 250 μl, containing Ag of 0.35 mg and Au of 0.53 mg; mice for control received injections of water with the same volume. Total number of mice was 80, which was divided into the following studies to address the a) distribution of Ag and Au by ICP-MS (16 mice, 4 mice per group), b) histological analysis and the renal function (creatinine (Cr) and creatine kinase (CK) status, 16 mice, 4 mice per group), c) TEM observation of kidney (12 mice, 3 mice per group), d) complement activation of serum (16 mice, 4 mice per group) and e) malondialdehyde (MDA) and superoxide dismutase (SOD) detection of subcutis and kidney (20 mice, 5 mice per group).

The protocol for animal experiment was reviewed and approved by the Institutional Review Board of Chinese Academy of Medical Sciences & Peking Union Medical College.

Determination of silver and gold content in tissues and organs by ICP-MS analysis

Mice in control and test groups were sacrificed on day 1 (24 h), day 8 and day 28 after injection of Au@Ag NRs. The tissues and organs were collected and frozen dried including brain, heart, lung, liver, spleen, kidney, bilateral axillary lymph nodes and subcutis tissue around Au@Ag NRs injection sites. The blood was collected from eye ball of the mice and frozen dried. The samples were further digested by weighting ~0.5 g dry tissue sample and adding it to 10 ml of a mixture of concentrated hydrochloric and nitric acid (1:3), followed by a microwave treatment of 20 min at 190°C, 70 bar. Microwave can provide a high-temperature, high-pressure environment that accelerates the digestion and dissolution of solid tissue samples in the acids. The final sample solutions were diluted to 40 ml deionised water.

The determination of total Ag and Au concentration in the solutions was analysed by ICP-MS (Thermo ICP-MS XII instrument, ThermoFisher) in bulk analysis mode. In our case, the standard curves for Au and Ag were prepared from 1 to 100 ppb and showed good linearity ($R^2 > 0.99$). The background value was always less than 0.1 ppb during the measurement. The sensitivity was high enough for our purpose. The intensity data obtained for the samples were corrected by those obtained for the blank. Quantification was performed by the external calibration. The amount of Ag and Au in different organs and tissues was given as percentage of the total injection dose.

Histological observation of subcutis tissue and organs

Mice in control and test groups were sacrificed on day 1, day 8 and day 28 post-injection. The tissues and organs were collected and fixed in 10% neutral buffered formalin including brain, heart, lung, liver, spleen, kidney, lymph node and subcutis tissue around Au@Ag NRs injection sites. After conventional processing, paraffin-embedded sections were stained with haematoxylin and eosin (H&E). The periodic

acid-Schiff (PAS) staining for kidney was also performed. After deparaffinisation and hydration, the sections of kidney were oxidised in 0.5% periodic acid solution for 5 min, followed by rinsing the sections in distilled water. Then the sections were placed in Schiff reagent for 15 min. Excess stain was removed with three 1-min washes by sodium metabisulphite solution, which were followed by distilled water wash for 2 min. The sections were counterstained in Mayer's haematoxylin for 1 min. The sections were examined using a microscope (BX53; Olympus) with a CCD camera (DP72; Olympus).

TEM observation of kidney tissue

Three mice of test and control groups, respectively, were anaesthetised with i.p. injection of 3% of pentobarbital sodium (Merck). After the anaesthesia, both left and right kidneys of the mice were isolated and quickly fixed within 1% v/v glutaraldehyde in 0.1 M sodium phosphate buffer (pH 7.2) overnight, washed by the same buffer and subsequently post-fixed in 1% w/v OsO_4 for 30 min. After being washed, the specimens were dehydrated in graded series of ethanol, transferred to propylene oxide and embedded in Epon-812. Ultrathin sections were cut, double-stained with uranyl acetate and lead citrate, and collected on copper meshwork. The sections were observed on a TEM (JEM-1010).

ELISA assay for measuring complement fractions 3, C3a and C5a

During the experiment, blood samples were collected from the eyes of the mice on days 1, 8 and 28 after s.c. injection of Au@Ag NRs. The blood samples were clotted at room temperature for 2 h and centrifuged at 3000 rpm for 30 min to separate the serum. The serum samples were stored at –80 °C for later use. Complement fraction 3 (C3) levels were measured using a commercially available C3 ELISA kit (R&D System). The C3a and C5a levels were also measured by mice C3a and C5a ELISA kit (Wuhan EIAab Science Co. Ltd) as according to the procedures described by the manufacturer's instructions.

SOD and MDA measurement in subcutis and kidney tissue

The subcutis tissue around the injection sites and kidney of the mice were homogenised in ice-cold normal saline (1:9 in ratio of w/v). The homogenates were centrifuged at 8000 × *g* for 15 min (4°C) and the supernatants were collected, the protein concentration were examined by Pierce® BCA protein assay kit and then stored at –80°C. The activities of SOD and the amount of MDA in the homogenates were examined by a kit (Cat. No. A003-4, MDA) purchased from Nanjing Jiancheng Bio-engineering Institute (Nanjing, China).

Blood biochemical parameter tests

Blood samples for blood biochemical parameter tests were collected at autopsy (tissue and organs were collected for histological analysis). Blood from Au@Ag NRs or control group was collected from the mice eyeballs, clotted and centrifuged at 3000 rpm for 30 min to obtain fresh serum samples. The serum biochemical measurement of Cr and CK was performed using an automated chemistry analyser (Olympus AU-5400, Mshima, Japan).

Statistical analysis

Data were expressed as means ± SD where indicated. Statistical differences were analysed using the two-sided Student's *t*-test. The $p < 0.05$ (*) and $p < 0.01$ (**) represent statistically significant difference.

Results

Physicochemical characterisations of gold NRs core/silver shell nanostructures (Au@Ag NRs)

The structural diagram of Au@Ag NRs is shown in Figure 1A. Most of the Au@Ag NRs were rod-like, and uniform in size and shape as shown in the representative images obtained from TEM (Figure 1B). The Au@Ag NRs was about 54 ± 7 nm in length and 18 ± 2 nm in diameter, having an average aspect ratio of 3 ± 0.5 (statistics from 154 NRs as shown in Figure S1). The Au@Ag NRs were synthesised using gold nanorods (AuNRs) as the template. The silver shell has a mean thickness of 1 nm (Figure 1B). The Au@Ag NRs exhibited a strong localised surface plasmon resonance peak at 703 nm which is different from original AuNRs (Figure 1C). The aqueous solutions of the Au@Ag NRs at different concentrations up to 80 pM were homogeneous and showed a light green colour (Figure 1D). The surface of the silver NR was negatively charged via electrostatic coating of PSS, with a Zeta potential of –47 mV, indicative of excellent stability (Figure 1E). By ICP-MS measurement, the molar ratio of silver to gold in Au@Ag NRs was 1.2, and relative weight of gold and silver was 66% and 34%, respectively.

Silver dynamic accumulation in the mice upon subcutaneous injection of the Au@Ag NRs

As stated in the introduction, the inert gold core can act as an internal reference and allows us to identify the silver of the injected Au@Ag NRs (stay with gold or leave after dissolved). After receiving single-dose subcutaneous injection, the mice were sacrificed at days 1, 8 and 28. Major organs including liver, kidney, lymph node, spleen, lung, heart and brain as well as subcutis around injection site were collected, and the amount of Ag and Au in the samples was quantified by ICP-MS (Table I). It is interesting to see that there were undetectable or extremely low levels of gold in the organs at each testing time point except for the subcutis and lymph nodes. The gold in subcutaneous tissue was high and relatively stable, which was 67.39% of injected amount on day 1, 64.57% on day 8 and 57.49% on day 28 after the injection. Meanwhile, gold in the lymph nodes was detected as 0.005%, 0.28% and 0.085% of injected amount on day 1, day 8 and day 28, respectively. In contrast, silver distribution in the organs and subcutis displayed a different pattern. Silver content in the subcutis decreased to 38.6% of the injected amount on day 1 after the injection, and followed continuous reduction on day 8 (7.9%) and day 28 (5.78%). Meanwhile, silver elevation referenced to the control was detected in the organs.

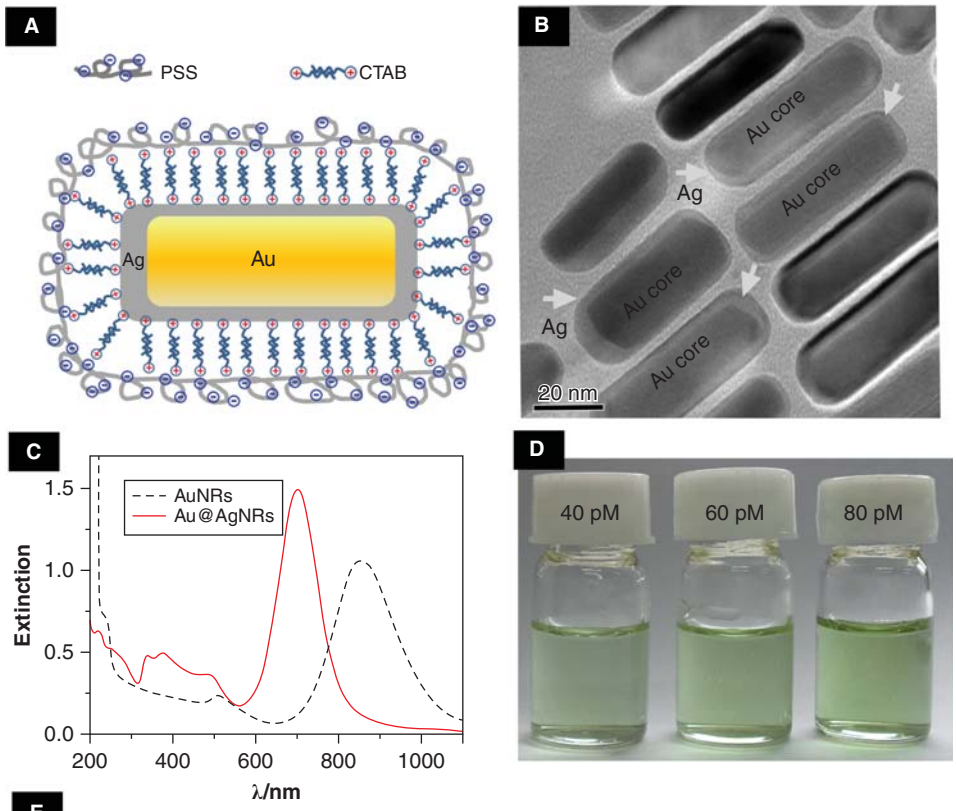

E

	Length (nm)	Width (nm)	ζ potential (mV)
Au@Ag NRs	54 ± 7	18 ± 2	–47.07 + 1.43

Figure 1. Physicochemical characterisations of the Au@Ag NRs. (A) Structural diagram of Au@Ag NRs; (B) TEM image; (C) UV–vis–NIR absorption spectra of Au@Ag NRs and original AuNRs; (D) photographs of aqueous suspensions at different NR concentrations; (E) Zeta potential and size distribution. The data were presented as mean ± SD (n = 3).

For kidney, there was an increasing accumulation of silver on day 28 post-injection, while at day 8 the level was similar to day 1. It should be noticed that the original molar ratio of Ag to Au in NR was 1.2, and that ratio was reduced to 0.628 on day 1, 0.134 on day 8 and 0.11 on day 28 in the subcutis. Taken above together, it is strongly suggested that the majority of the injected Au@Ag NRs was aggregated in the subcutis of injection site, and the silver shell was dissolved rapidly to release silver ions, and the latter then diffused to different organs. Evidently, it was hard to identify any rod-like materials in the H&E-stained sections of the organs. Instead, a large amount of the Au@Ag NRs was seen aggregated in the subcutis (Figure 2), which meant that the silver content in the organs was mainly attributed to the silver shell dissolution. Meanwhile, small amount of the Au@Ag NRs migrated into lymph nodes as low amount of gold was detected. One point needed to explain is that only 67% of originally injected Au was detected in the subcutis instead of 100%. The low

Table I. Silver and gold distribution in the organs of mice that received subcutaneous injection of AgNRs analysed by ICP-MS[1] (16 mice, 4 mice per group); the data were presented as mean ± SD (number of mice in each group). Both silver and gold in the control group were measured, and the values were not detectable.

	Day 1		Day 8		Day 28	
Tissues	Ag[2]	Au[2]	Ag[2]	Au[2]	Ag[2]	Au[2]
Subcutis	38.581 ± 1.893 (4)	67.389 ± 0.757 (4)	7.901 ± 2.051 (4)	64.568 ± 2.666 (4)	5.778 ± 1.910 (4)	57.489 ± 5.413 (4)
Liver	4.164 ± 0.948 (4)	ND[3]	3.452 ± 0.844 (4)	0.007 ± 0.003 (4)	1.404 ± 0.517 (4)	0.117 ± 0.058 (4)
Spleen	0.034 ± 0.006 (4)	ND	0.186 ± 0.064 (4)	0.001 ± 0.001 (4)	0.104 ± 0.001 (4)	0.010 ± 0.001 (4)
Lung	0.035 ± 0.017 (4)	ND	0.047 ± 0.036 (4)	0.001 ± 0.001 (4)	0.050 ± 0.006 (4)	0.005 ± 0.002 (4)
Kidney	0.009 ± 0.004 (4)	ND	0.009 ± 0.002 (4)	ND	0.017 ± 0.004 (4)	0.003 ± 0.001 (4)
Heart	0.012 ± 0.007 (4)	ND	0.021 ± 0.010 (4)	0.001 ± 0.0002 (4)	0.019 ± 0.006 (4)	0.012 ± 0.006 (4)
Brain	0.037 ± 0.029 (4)	ND	0.063 ± 0.008 (4)	ND	0.140 ± 0.108 (4)	0.001 ± 0.001 (4)
Lymph nodes[4]	0.009 ± 0.009 (4)	0.005 ± 0.006 (4)	0.035 ± 0.022 (4)	0.280 ± 0.021 (4)	0.078 ± 0.023 (4)	0.085 ± 0.029 (4)

[1]In our case, the standard curves for Au and Ag were prepared from 1 to 100 ppb and showed good linearity (R^2 > 0.99). The back ground value was always less than 0.1 ppb during the measurement; [2]Percentage of injection dose in mass ratio (total amount of Ag and Au subcutaneously injected to a mouse were 0.35 and 0.53 mg, respectively); [3]Not detectable; [4]The bilateral axillary lymph nodes were collected and used for the measurement of Ag and Au by ICP-MS.

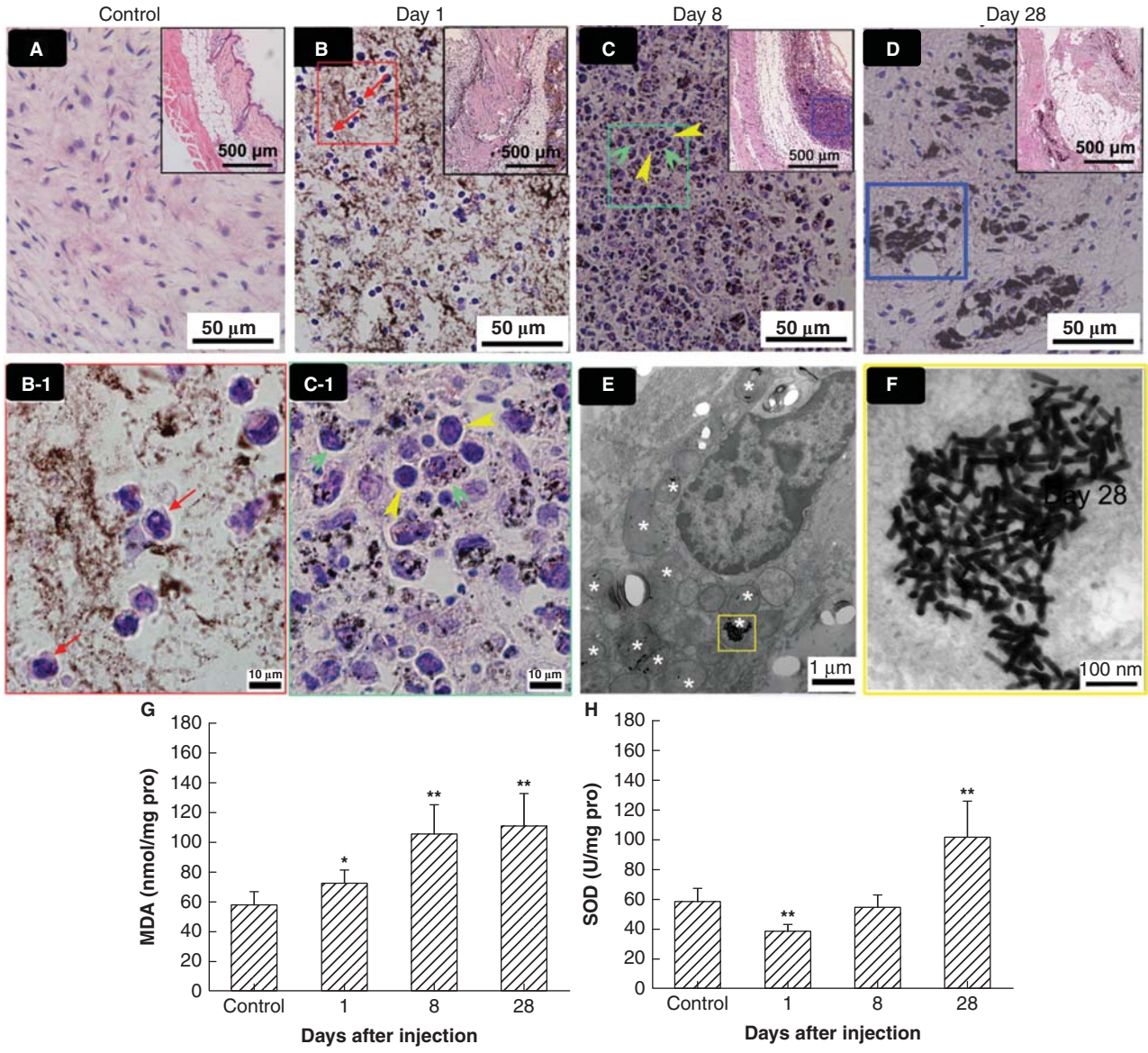

Figure 2. Time-dependent effects of Au@Ag NRs on the subcutis tissue around the injection site for the BALB/c mice. (A) H&E staining of subcutis tissue of control mice (4 mice); (B–D) H&E staining of subcutis tissue of Au@Ag NR-injected mice on days 1, 8 and 28 (12 mice, 4 mice for each group); (B-1) and (C-1) magnification of (B) and (C), respectively; (E) TEM observation of subcutis around the injection site of the mice on day 28 (3 mice), white star indicated lysosomes and phagosomes in the macrophage cell; (F) magnification of (G), showing Au@Ag NRs aggregate in the cells; (G) and (H) MDA production and SOD activity in the homogenates of the subcutis tissues, respectively (20 mice, 5 mice per group), data were presented as mean ± SD ($n = 5$). The * represents significant difference from sample groups to the control group (*$p < 0.05$, **$p < 0.01$). Red arrow points to neutrophils, yellow arrow head points to lymphocytes, and green arrow points macrophage cells.

recovery ratio is probably due to the technical limitations of sample collection.

Interaction of Au@Ag NRs to the subcutis tissue of injection site

When the Au@Ag NRs were injected into the subcutaneous tissue, they induced a typical inflammatory process as shown in Figure 2A–D. On day 1 post-injection, large amounts of Au@Ag NRs were seen in brown and mainly dispersed in interstitial structures of the subcutis, little was seen in cells. Meanwhile, inflammatory cells including neutrophils (pointed by red arrow) and lymphocytes (pointed by yellow arrow head) were recruited and infiltrated into the area, indicating that acute inflammatory reactions occurred. On day 8, in some areas dense Au@Ag NRs were observed, along with influx of macrophages engulfing Au@Ag NRs and becoming dark brown (pointed by green arrow head); also, more lymphocytes were infiltrating to the area, suggesting that inflammatory reactions became stronger. On day 28, dense aggregates of the Au@Ag NRs were seen in the tissue while lymphocytes were rarely seen, and slight fibrosis could be observed as pink rope-like structures, which indicated that the inflammatory process went to end. To confirm that the aggregates are composed of Au@Ag NRs, the subcutis sample on day 28 post-injection was also analysed with TEM (Figure 2E), and the observation clearly indicated that lots of the NRs were stayed in the subcutis. It was seen from Figure 2E and F that the Au@Ag NRs were taken up by cells in the subcutis. According to the nuclear morphology, the cells that engulfed Au@Ag NRs are macrophage

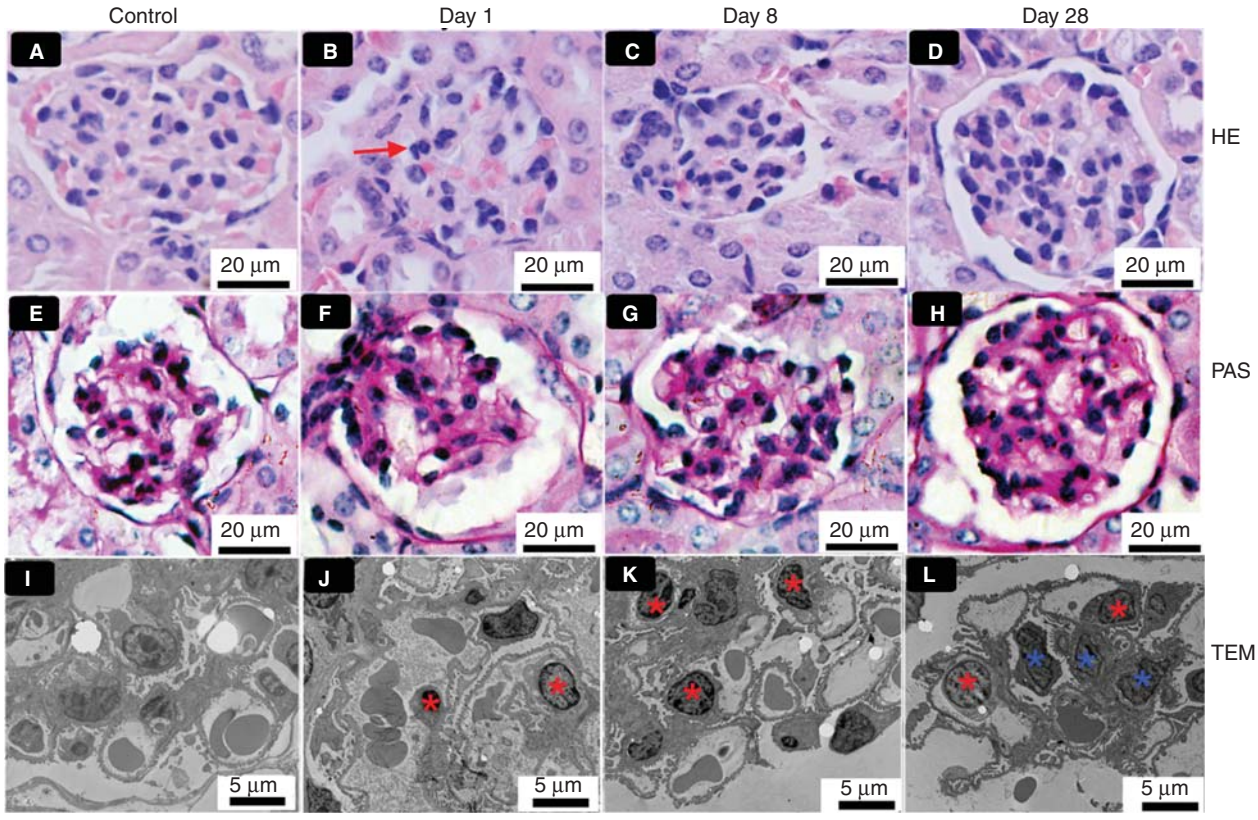

Figure 3. Morphological variation of glomerulus for the mice within 28 days after subcutaneous injection of Au@Ag NRs using histological staining (16 mice, 4 mice per group) and TEM observation (12 mice, 3 mice per group). (A–D) H&E staining; (E–H) PAS staining; (I–L) TEM observations. Red star indicates inflammatory cells in the blood vessels in the glomerulus. Blue star indicates mesangial cell in the glomerulus. Red arrow points to neutrophils.

cells. Many Au@Ag NRs stayed in the vesicles (pointed by white star) of the macrophage cell. In the above inflammatory process, a product of membrane lipid peroxidation, MDA, in the subcutis around the injection site was also significantly increased (Figure 2F), suggesting that the subcutaneously injected Au@Ag NRs induced oxidative stress of the cells. SOD is a biomarker of antioxidant defence of cells; the activities of SOD in the subcutis were decreased on day 1 post Au@Ag NRs injection, evidencing the Au@Ag NR-induced oxidative stress of the cells, and the SOD level then went up gradually, suggesting that the subcutis tissue was in a stressful status to produce a large amount of SOD against the oxidative damage (Figure 2G).

Kidney injury of mice receiving Au@Ag NRs injection and possible mechanisms

We next investigated whether the subcutaneous injection of Au@Ag NRs had impacts on the kidney since it has been reported that kidney is the first target organ of heavy metal toxicity (Bigazzi 1999) and there was an increasing accumulation of silver in the kidney on day 28 post-injection in the current study. As shown in the top (H&E stained) of Figure 3, the morphology of glomerulus in the kidney was affected significantly when mice received the subcutaneous administration of Au@Ag NRs. On day 1 and day 8 post-injection, the glomerulus lost their normal morphology; in particular the wall layer composed of parietal epithelium was damaged on day 1. Although the glomerulus shape became similar to that of control on day 28, the morphology did not recover to the normal, and the glomerulus looked like more "solid", and capillary lumen seemed to be reduced. When using PAS to specifically stain collagen in the glomerulus basement membrane, the basic change appeared was diffuse thickening of basement membrane (middle in Figure 3). The glomerulus in the control group appeared normal, with a thin basement membrane (in rose-pink colour), while the glomerulus in Au@Ag NRs group appeared to have diffuse thickening of the basement membrane, particularly on day 28 post-injection. TEM images of the glomerulus (bottom in Figure 3) provided further detail evidence that the wall layer composed of parietal epithelium that disappeared on day 1. Additionally, it could be noticed that more inflammatory cells were seen in the vessels on day 1 and day 8 (red star labelled), indicating that inflammatory reactions occurred, and on day 28 more mesangial cells (blue star labelled) appeared while the inflammatory cells reduced, indicating that the inflammatory process went to end and suggesting that glomerulus basement membrane was possibly affected.

TEM images with high magnification provided more variations of glomerulus in detail (Figure 4). The apparent change of the glomerulus on day 1 (Figure 4B) was large amounts of protein-like substances appearing in the capillary lumen (circled by red line), indicating that acute inflammatory reactions occurred in the kidney. The protein-like substance reduced over time. Diffuse loss of foot

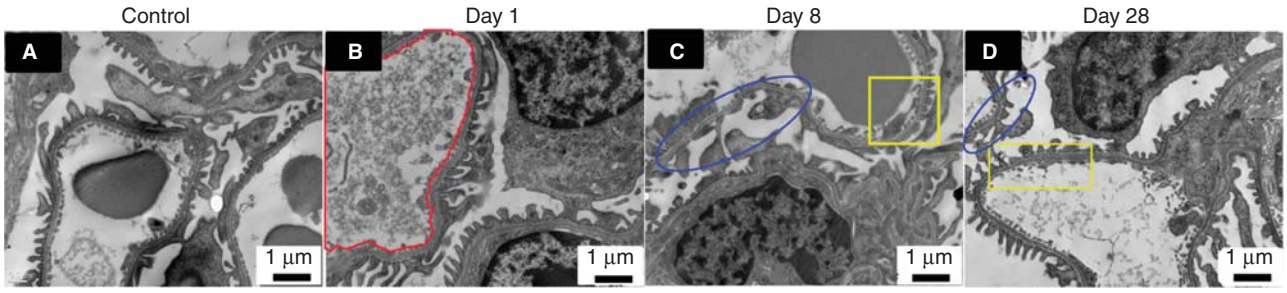

Figure 4. TEM images of kidney glomerulus for the mice within 28 days after subcutaneous injection of Au@Ag NRs (12 mice, 3 mice per group). (A) Control; (B) Au@Ag NR-injected mice on day 1; (C) Au@Ag NR-injected mice on day 8; (D) Au@Ag NR-injected mice on day 28. Red circle indicates the protein-like substances appearing in the capillary lumen. Blue circle indicates the diffuse loss of foot processes of visceral epithelial cells. Yellow rectangle indicates endothelial cells detachment.

processes of visceral epithelial cells was seen on days 8 and 28 (circled by blue line); additionally, endothelial cells detachment could be observed (in yellow rectangle). The Au@Ag NRs also induced morphological changes with the renal tubule with the proximal renal tubule's mitochondria swelling on day 28 post-injection (Figure S5), implying that we should also be alert to the influence of Au@Ag NRs on renal tubule's function.

It has been reported that membranous nephropathy is closely associated with immune responses induced by heavy metals either present in the environment or administered for therapeutic reasons (Bigazzi 1999). By ICP-MS measurement, we determined that silver content in the blood was 0.631 ± 0.10 μg/ml, and gold was 0.016 ± 0.004 μg/ml, implying that Ag^+ dissolved from Au@Ag NRs entered into the circulating blood. In blood, complement system is one of the crucial immune defences of human and composed of more than 30 kinds of proteins. C3 is the most abundant complement protein and plays a pivotal role in all three complement pathways. The subcutaneous administration of Au@Ag NRs induced a sharp increase of C3 on day 1 followed by a significant consumption (Figure 5A–C), indicating that acute inflammatory reactions occurred and eliminated gradually. According to the C3 consumption, cleavage products C3a and C5a were upregulated in the serum significantly. These evidenced that the complement system was activated. It has been well established that C5a can recruit neutrophils to produce oxidants that could interact with the kidney cells. As shown in Figure 3, neutrophils were seen in the kidney tissue (pointed by red arrows). Besides, Ag^+ itself could also interact with the kidney cells and induced cell membrane

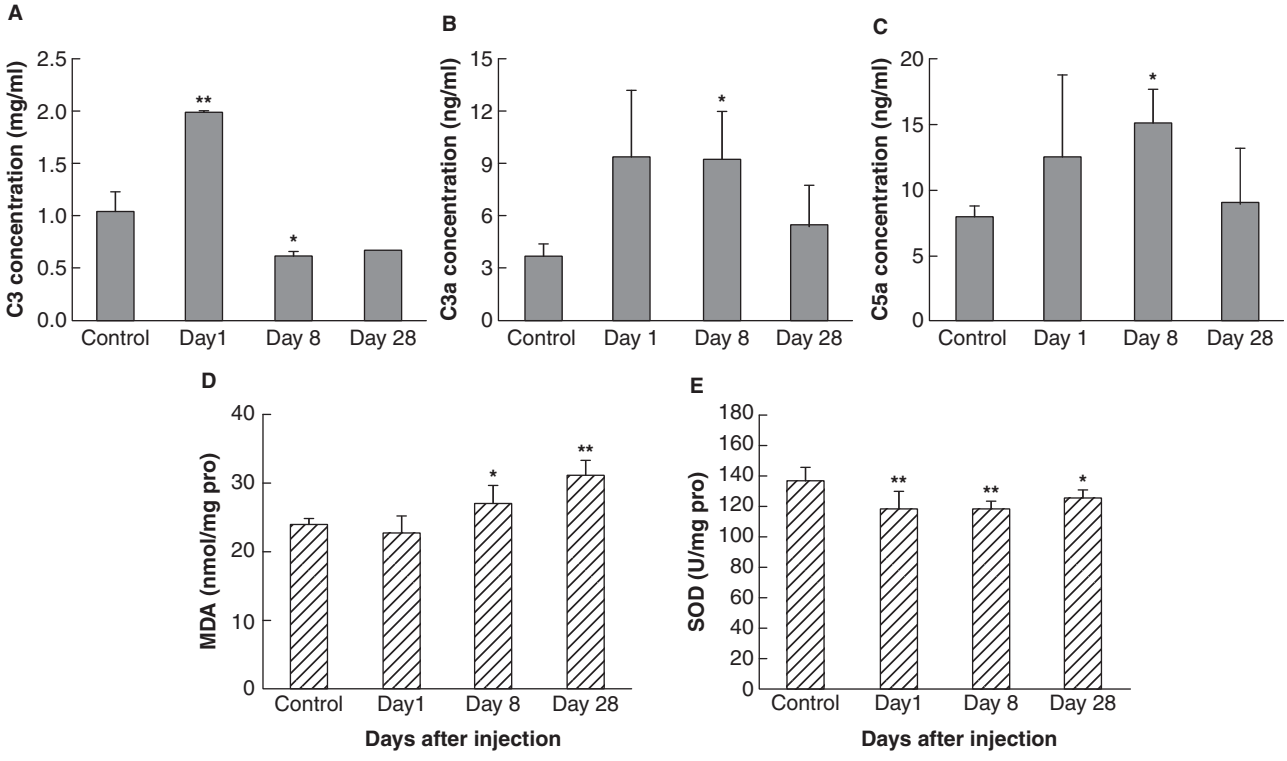

Figure 5. Immune responses induced by subcutaneous injection of Au@Ag NRs. (A–C) Variation of complement fraction C3, C3a and C5a in the serum of mice that received Au@Ag NRs injection (16 mice, 4 mice per group), data were presented as mean ± SD ($n = 4$). (D) and (E) MDA production and SOD activity of kidney homogenates, respectively (20 mice, 5 mice per group), data were presented as means ± SD ($n = 5$). The * represents significant difference from sample groups to the control group (*$p < 0.05$, **$p < 0.01$).

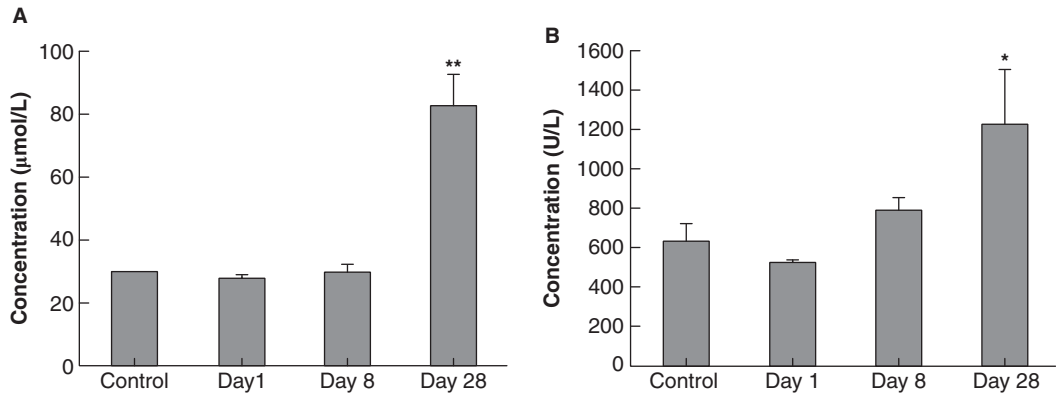

Figure 6. Subcutaneously injected Au@Ag NRs affected filtration function of the kidney. Cr (A) and CK (B) in the serum of mice that received Au@AgNRs injection (16 mice, 4 mice per group) were presented as means ± SD ($n = 4$). The * represents significant difference from sample groups to the control group (*$p < 0.05$, **$p < 0.01$).

oxidation (Cheng et al. 2013). Both the oxidants and Ag^+ synergised to induce kidney oxidative damage that was evidenced by the elevated MDA level in the homogenates of kidney tissue and down-regulated SOD activity in a time-dependent manner (Figure 5D–E).

As Au@Ag NR-induced morphological changes were mainly associated with glomerulus basement membrane, it implied that filtration function of the kidney was affected. Therefore, serum biochemical parameters Cr and CK were examined within the experimental period (Figure 6). Both parameters are associated with the kidney's filtration function, and they cannot be clinically detected until majority of the glomeruli are damaged and the filtration efficacy is reduced more than 50%. In the present study, Cr and CK showed a significant increase on the day 28 post-injection, indicating that the glomerular filtration was affected significantly. These variations were consistent with the pathological observations.

Discussion

As mentioned above, there was increase in silver and no Au@Ag NRs detected in the kidney on day 28 post-injection, while glomerulus morphology and kidney filtration function changed significantly, along with the levels of MDA and SOD up-regulated. This strongly suggests that the observed kidney toxicity was attributed to the silver ions released from the Au@Ag NRs. Here we would like to further discuss two points.

First, it should be mentioned that in our study, each 250 μl NRs suspension contains 19 μg bound CTAB and 16 μg free CTAB (Figure S2). CTAB is a detergent that can interact with cell membranes. Although rare results on subcutaneous administration of CTAB are reported, toxicological data obtained from i.p. injection provide useful reference. For example, the acute i.p. LD50 of CTAB for female mice was 106 mg/kg. If average weight is 20 g per mouse, the LD50 for one mouse is 2.1 mg (Isomaa & Ekman 1975). Additionally, CTAB can be metabolised fast. As described by the manufacturer of CTAB (AMRESCO), the amount of radioactivity in liver declined from 39% to 2% after i.p. injection for 24 h.

To identify the effect of subcutaneously injected CTAB on filtration function of kidney, we conducted two additional experiments: one is to determine total CTAB in the solution for the subcutaneous injection; the other is injecting 35 μg of CTAB to each mouse subcutaneously. Results showed that the subcutaneous administration did not induce significant variation of CK and Cr levels in the serum within 28 days post-injection (Figure S3). Taken together, CTAB in the solution of Au@Ag NRs did not cause toxic effects on the kidney. In addition, subcutaneously injected CTAB did not induce obvious inflammation reaction in the subcutis of the injection site (Figure S4).

Second, in kidneys, deposition of silver has been reported to occur in the renal glomerular basement membrane, and in the mesangium (Danscher 1981; Ham & Tange 1972; Moffat & Creasev 1972; Day et al. 1976); however, there was no observable silver deposition in the kidney in the current case. The reason is likely that the injected dose was quite low and the administration was different compared with those in the literatures that reported silver deposition. For instances, Genter et al. reported that aggregated Ag-NPs were observed in the kidney of mice that received intranasal administration of 25-nm AgNP with ~2 or 10 mg per mouse (Genter et al. 2012). Ernst et al. demonstrated the deposition of silver in kidneys of rat given a single intravenous injection of radiolabelled $AgNO_3$ with 0.5 mg Ag per rat (Ernst et al. 1991). Tiwari et al. studied dose-dependent *in vivo* toxicity assessment of silver in Wistar rat. Four different doses of AgNPs (4, 10, 20 and 40 mg/kg) were injected intravenously. Silver particle deposition was only found in the highest dose group of 40 mg/kg, and the concentration of the accumulated silver in the kidney reached 3.34 ± 0.1 μg (Tiwari et al. 2011). In our study, subcutaneous administration was used instead of intravenous one, which allows less silver to enter into the blood and the kidney. Besides, the injection dose of Ag was 17.5 mg/kg, and the silver in the kidney was only 0.595 ± 0.014 μg on 28 days post-injection, which is much lower than that reported by Tiwari et al. Therefore, silver deposition is hardly observed in the kidney due to the low dose and the subcutaneous administration way.

We also would like to address the advantages of Au@Ag NRs in the toxicity research of silver NPs. Different from other metal NPs, silver NPs can release silver ions readily in water or in the culture medium, which has been evidenced by the literatures (Kittler et al. 2010; McQuillan et al. 2012; Xiu et al. 2012). This performance has given complexity to the toxic effects of silver NPs. One controversial issue is that whether silver NPs or silver ions dissolution from the silver NP exert toxicity of the silver NPs, because using conventional measurement such as ICP-MS cannot identify silver ions and silver NPs in the cells or tissues. The novel nanostructure of gold NR core/silver shell provided the way of directly determining silver NPs or silver ions distribution in the cells or tissues. The gold NR core also allowed us to identify whether NPs migrated to other tissues or organs from the original injection site. It could be determined using this novel nanostructure that a small amount of Au@Ag NRs migrated into the lymph nodes. Lymph node is likely to be a target organ for subcutaneously administrated NPs, because there are plenty of lymphatic vessels in the subcutaneous tissue for NP transportation. We previously observed small amounts of multi-walled carbon nanotubes migrated into the lymph nodes of mice that received subcutaneous injection of the carbon nanotubes (Meng et al. 2011). Other group also reported that lymph nodes collected a high number of gold NPs (Carr et al. 1996). In our case, the level was quite low, and only 0.28% of injected Au@Ag NRs migrated into the lymph nodes.

Nevertheless, it was hard to identify the toxic effects of Au@Ag NRs or silver ions on the subcutaneous tissue directly, because there were Au@Ag NRs and silver ions existing in the injection site. We previously demonstrated that it was the released Ag^+ that caused membrane damage of the fibroblast cells and induced cell apoptosis (Cheng et al. 2013). According to the data that Au@Ag NRs were dissolved rapidly in the subcutaneous tissue, herein we would suggest that the oxidative damage of the subcutis was mainly attributed to the Au@Ag NRs dissolution and Ag^+ release.

Conclusion

Taken together, the subcutaneously administrated Au@Ag NRs mainly aggregated in the subcutis around the injection site, while small amount of the Au@Ag NRs migrated into the lymph nodes of the mice. The Au@Ag NRs were dissolved rapidly in the subcutaneous tissue and released large amounts of silver ions that diffused to the organs including kidney, liver, spleen, lung, heart and brain. The silver ions induced complement activation as well as interacted directly with the cell membranes, which resulted in induced kidney oxidative damage and eventually led to the morphological changes and filtration function impairment of the glomerulus. The released silver ions also caused oxidative injury of subcutaneous tissue in the injection site. Our research results strongly suggest that when using silver NPs for wound dressing, safety consideration for administration and dosage is very important, and caution should be taken for potential toxic effects.

Acknowledgement

The authors thank for the financial support from National Key Basic Research Program of China (2011CB933504, 2011CB932802 and 2010CB934002).

Declaration of interest

The authors report no conflicts of interest. The authors alone are responsible for the content and writing of the paper.

References

Ahamed M, Alsalhi MS, Siddiqui MK. 2010. Silver nanoparticle applications and human health. Clin Chim Acta 411:1841–1848.

Austin LA, Kang B, Yen CW, El-Sayed MA. 2011. Nuclear targeted silver nanospheres perturb the cancer cell cycle differently than those of nanogold. Bioconjug Chem 22:2324–2331.

Babu MM, Sridhar J, Gunasekaran P. 2011. Global transcriptome analysis of Bacillus cereus ATCC 14579 in response to silver nitrate stress. J Nanobiotechnol 9:49.

Bigazzi PE. 1999. Metals and kidney autoimmunity. Environ Health Perspect 107:753–765.

Braydich-Stolle LK, Lucas B, Schrand A, Murdock RC, Lee T, Schlager JJ, et al. 2010. Silver nanoparticles disrupt GDNF/Fyn kinase signaling in spermatogonial stem cells. Toxicol Sci 116: 577–589.

Carr KE, Hazzard RA, Reid S, Hodges GM. 1996. The effect of size on uptake of orally administered latex microparticles in the small intestine and transport to mesenteric lymph nodes. Pharm Res 13:1205–1209.

Chaloupka K, Malam Y, Seifalian AM. 2010. Nanosilver as a new generation of nanoproduct in biomedical applications. Trends Biotechnol 28:580–588.

Cheng XL, Zhang WQ, Ji YL, Meng J, Guo H, Liu J, et al. 2013. Revealing silver cytotoxicity using Au nanorods/Ag shell nanostructures: disrupting cell membrane and causing apoptosis through oxidative damage. RSC Adv 3:2296–2305.

Cohen MS, Stern JM, Vanni AJ, Kelley RS, Baumgart E, Field D, et al. 2007. In vitro analysis of a nanocrystalline silver-coated surgical mesh. Surg Infect (Larchmt) 8:397–403.

Comfort KK, Maurer EI, Braydich-Stolle LK, Hussain SM. 2011. Interference of silver, gold, and iron oxide nanoparticles on epidermal growth factor signal transduction in epithelial cells. ACS Nano 5:10000–10008.

Damm C, Munstedt H. 2008. Kinetic aspects of the silver ion release from antimicrobial polyamide/silver nanocomposites. Appl Phys A Mater Sci Process 91:479–486.

Danscher G. 1981. Light and electron microscopic localization of silver in biological tissue. Histochemistry 71:177–186.

Day WA, Hunt JS, McGiven AR. 1976. Silver deposition in mouse glomeruli. Pathology 8:201–204.

Edwards-Jones V. 2009. The benefits of silver in hygiene, personal care and healthcare. Lett Appl Microbiol 49:147–152.

Ernst E, Rungby J, Baatrup E. 1991. Ultrastructural localization of silver in rat testis and organ distribution of radioactive silver in the rat. J Appl Toxicol 11:317–321.

Eom HJ, Choi J. 2010. p38 MAPK activation, DNA damage, cell cycle arrest and apoptosis as mechanisms of toxicity of silver nanoparticles in Jurkat T cells. Environ Sci Technol 44:8337–8342.

Florea AM, Busselberg D. 2006. Occurrence, use and potential toxic effects of metals and metal compounds. Biometals 19:419–427.

Genter MB, Newman NC, Shertzer HG, Ali SF, Bolon B. 2012. Distribution and systemic effects of intranasally administered 25 nm silver nanoparticles in adult mice. Toxicol Pathol 40:1004–1013.

Hackenberg S, Scherzed A, Kessler M, Hummel S, Technau A, Froelich K, et al. 2011. Silver nanoparticles: evaluation of DNA damage, toxicity and functional impairment in human mesenchymal stem cells. Toxicol Lett 201:27–33.

Ham KN, Tange JD. 1972. Silver deposition in rat glomerular basement membrane. Aust J Exp Biol Med Sci 50:423–434.

Isomaa B, Ekman K. 1975. Embryotoxic and teratogenic effects of CTAB, a cationic surfactant, in the mouse. Food Cosmet Toxicol 13:331–334.

Johnston HJ, Hutchison G, Christensen FM, Peters S, Hankin S, Stone V. 2010. A review of the in vivo and in vitro toxicity of silver

and gold particulates: particle attributes and biological mechanisms responsible for the observed toxicity. Crit Rev Toxicol 40:328–346.
Kang SJ, Ryoo IG, Lee YJ, Kwak MK. 2012. Role of the Nrf2-heme oxygenase-1 pathway in silver nanoparticle-mediated cytotoxicity. Toxicol Appl Pharmacol 258:89–98.
Kim WY, Kim J, Park JD, Ryu HY, Yu IJ. 2009. Histological study of gender differences in accumulation of silver nanoparticles in kidneys of Fischer 344 rats. J Toxicol Environ Health A 72:1279–1284.
Kittler S, Greulich C, Diendorf J, Koller M, Epple M. 2010. Toxicity of silver nanoparticles increases during storage because of slow dissolution under release of silver ions. Chem Mater 22:4548–4554.
Korani M, Rezayat SM, Gilani K, Arbabi Bidgoli S, Adeli S. 2011. Acute and subchronic dermal toxicity of nanosilver in guinea pig. Int J Nanomedicine 6:855–862.
Lankveld DP, Oomen AG, Krystek P, Neigh A, Troost-de Jong A, Noorlander CW, et al. 2010. The kinetics of the tissue distribution of silver nanoparticles of different sizes. Biomaterials 31:8350–8361.
Lee YS, Kim DW, Lee YH, Oh JH, Yoon S, Choi MS, et al. 2011. Silver nanoparticles induce apoptosis and G2/M arrest via PKCzeta-dependent signaling in A549 lung cells. Arch Toxicol 85:1529–1540.
Li PW, Kuo TH, Chang JH, Yeh JM, Chan WH. 2010. Induction of cytotoxicity and apoptosis in mouse blastocysts by silver nanoparticles. Toxicol Lett 197:82–87.
Maneewattanapinyo P, Banlunara W, Thammacharoen C, Ekgasit S, Kaewamatawong T. 2011. An evaluation of acute toxicity of colloidal silver nanoparticles. J Vet Med Sci 73:1417–1423.
Mcquillan JS, Groenaga Infante H, Stokes E, Shaw AM. 2012. Silver nanoparticle enhanced silver ion stress response in Escherichia coli K12. Nanotoxicology 6:857–866.
Meng J, Yang M, Jia FM, Xu Z, Kong H, Xu HY. 2011. Immune responses of BALB/c mice to subcutaneously injected multi-walled carbon nanotubes. Nanotoxicology 5:583–591.
Miura N, Shinohara Y. 2009. Cytotoxic effect and apoptosis induction by silver nanoparticles in HeLa cells. Biochem Biophys Res Commun 390:733–737.
Moffat DB, Creasev M. 1972. The distribution of ingested silver in the kidney of the rat and of the rabbit. Acta Anat (Basel) 83:346–355.
Nallathamby PD, Xu XH. 2010. Study of cytotoxic and therapeutic effects of stable and purified silver nanoparticles on tumor cells. Nanoscale 2:942–952.
Park EJ, Bae E, Yi J, Kim Y, Choi K, Lee SH, et al. 2010. Repeated-dose toxicity and inflammatory responses in mice by oral administration of silver nanoparticles. Environ Toxicol Pharmacol 30:162–168.
Piao MJ, Kang KA, Lee IK, Kim HS, Kim S, Choi JY, et al. 2011a. Silver nanoparticles induce oxidative cell damage in human liver cells through inhibition of reduced glutathione and induction of mitochondria-involved apoptosis. Toxicol Lett 201:92–100.
Piao MJ, Kim KC, Choi JY, Choi J, Hyun JW. 2011b. Silver nanoparticles down-regulate Nrf2-mediated 8-oxoguanine DNA glycosylase 1 through inactivation of extracellular regulated kinase and protein kinase B in human Chang liver cells. Toxicol Lett 207:143–148.
Sanpui P, Chattopadhyay A, Ghosh SS. 2011. Induction of apoptosis in cancer cells at low silver nanoparticle concentrations using chitosan nanocarrier. ACS Appl Mater Interfaces 3:218–228.
Singh SK, Goswami K, Sharma RD, Reddy MV, Dash D. 2012. Novel microfilaricidal activity of nanosilver. Int J Nanomedicine 7:1023–1030.
Sondi I, Salopek-Sondi B. 2004. Silver nanoparticles as antimicrobial agent: a case study on E. coli as a model for gram-negative bacteria. J Colloid Interface Sci 275:177–182.
Teodoro JS, Simoes AM, Duarte FV, Rolo AP, Murdoch RC, Hussain SM, et al. 2011. Assessment of the toxicity of silver nanoparticles in vitro: a mitochondrial perspective. Toxicol In Vitro 25:664–670.
Tiwari DK, Jin T, Behari J. 2011. Dose-dependent in-vivo toxicity assessment of silver nanoparticle in Wistar rats. Toxicol Mech Methods 21:13–24.
van der Zande M, Vandebriel RJ, Van Doren E, Kramer E, Herrera Rivera Z, Serrano-Rojero CS, et al. 2012. Distribution, elimination, and toxicity of silver nanoparticles and silver ions in rats after 28-day oral exposure. ACS Nano 6:7427–7442.
Wijnhoven SWP, Peijnenburg WJGM, Herberts CA, Hagens WI, Oomen AG, Heugens EHW, et al. 2009. Nano-silver - a review of available data and knowledge gaps in human and environmental risk assessment. Nanotoxicology 3:109–U78.
Xiang YU, Wu XC, Liu DF, Li ZY, Chu WG, Feng LL, et al. 2008. Gold nanorod-seeded growth of silver nanostructures: From homogeneous coating to anisotropic coating. Langmuir 24:3465–3470.
Xiu ZM, Zhang QB, Puppala HL, Colvin VL, Alvarez PJ. 2012. Negligible particle-specific antibacterial activity of silver nanoparticles. Nano Lett 12:4271–4275.
Zook JM, Long SE, Cleveland D, Geronimo CL, Maccuspie RI. 2011. Measuring silver nanoparticle dissolution in complex biological and environmental matrices using UV-visible absorbance. Anal Bioanal Chem 401:1993–2002.

Supplementary material available online

Supplementary Figures S1–S5.